

Generalization with quantum geometry for learning unitaries

Tobias Haug^{1,*} and M. S. Kim¹

¹*QOLS, Blackett Laboratory, Imperial College London SW7 2AZ, UK*

Generalization is the ability of quantum machine learning models to make accurate predictions on new data by learning from training data. Here, we introduce the data quantum Fisher information metric (DQFIM) to determine when a model can generalize. For variational learning of unitaries, the DQFIM quantifies the amount of circuit parameters and training data needed to successfully train and generalize. We apply the DQFIM to explain when a constant number of training states and polynomial number of parameters are sufficient for generalization. Further, we can improve generalization by removing symmetries from training data. Finally, we show that out-of-distribution generalization, where training and testing data are drawn from different data distributions, can be better than using the same distribution. Our work opens up new approaches to improve generalization in quantum machine learning.

The key challenge in quantum machine learning is to design models that can learn from data and apply their acquired knowledge to perform well on new data [1]. This latter ability is called generalization and has been intensely studied recently [2–17]. Constructing models that generalize well is essential for quantum machine learning tasks such as variational learning of unitaries [18–24], which is applied to unitary compiling [11, 25, 26], quantum simulation [10, 27, 28], quantum autoencoders [29, 30] and black-hole recovery protocols [31].

However, a priori it is difficult to predict whether a given quantum machine learning model will be able to generalize and usually time-consuming numerical studies have to be performed. This is further confounded by the fact that the training of quantum machine learning models is usually hard [32–36] and requires careful design to succeed [32, 33, 37–39].

Thus, a metric that quantitatively predicts both training success and generalization is essential to aid the quest for better quantum machine learning models [8, 40–49] and potential advantages over classical models [50–53]. In classical machine learning, measures of capacity have been developed which can directly evaluate generalization [4, 5, 54–56]. Recent works proposed the quantum Fisher information metric to measure the capacity of parameterized quantum states [37, 48, 57, 58], however a connection with generalization has not been established.

Here, we introduce the data quantum Fisher information metric (DQFIM) to predict the performance of quantum machine learning models for learning unitaries. Given an ansatz circuit and training data, the rank of the DQFIM quantifies the circuit depth and amount of data needed for generalization and convergence to a global minimum of the cost function. We apply the DQFIM to reduce the cost of generalization by finding models which require a low number of training data. Further, out-of-distribution generalization, i.e. the training data is drawn from a different distribution than the

test data, can exhibit better performance compared to in-distribution generalization. Finally, while symmetries can reduce complexity, they can also hinder generalization. Our measure provides a practical way to understand the generalization capability of quantum machine learning models and guides the design of better models.

Model.— Let us consider a target unitary V , which we want to approximate with ansatz unitary $U(\boldsymbol{\theta})$ parameterized by M -dimensional parameter vector $\boldsymbol{\theta}$. We learn from a training set $S_L = \{|\psi_\ell\rangle, V|\psi_\ell\rangle\}_{\ell=1}^L$ of L states which are randomly drawn from a distribution of states $|\psi_\ell\rangle \in W$ [10, 28, 59]. We learn by minimizing the cost function given by the fidelity

$$C_{\text{train}}(\boldsymbol{\theta}, S_L) = 1 - \frac{1}{L} \sum_{\ell=1}^L |\langle \psi_\ell | V^\dagger U(\boldsymbol{\theta}) | \psi_\ell \rangle|^2, \quad (1)$$

which can be efficiently measured with the SWAP test [60]. This model generalizes when the learned unitary correctly transforms any state sampled from W which is evaluated with the test error

$$C_{\text{test}}(\boldsymbol{\theta}, W) = 1 - \mathbb{E}_{|\psi\rangle \in W} [|\langle \psi | V^\dagger U(\boldsymbol{\theta}) | \psi \rangle|^2]. \quad (2)$$

In variational quantum algorithms [20] and quantum control [61], the parameterized ansatz unitary $U(\boldsymbol{\theta}) = \prod_{k=1}^G U^{(k)}(\boldsymbol{\theta}_k)$ commonly consists of G repeating layers of unitaries $U^{(k)}(\boldsymbol{\theta}_k) = \prod_{n=1}^K \exp(-i\boldsymbol{\theta}_{kn} H_n)$, where H_n are hermitian operators, $\boldsymbol{\theta}_k$ a K -dimensional vector, and $\boldsymbol{\theta} = \{\boldsymbol{\theta}_1, \dots, \boldsymbol{\theta}_G\}$ the $M = GK$ dimensional parameter vector. The optimization program starts with a randomly chosen $\boldsymbol{\theta}$ and iteratively minimizes Eq. (1) with the gradient $\nabla C_{\text{train}}(\boldsymbol{\theta})$, which can be efficiently estimated by a quantum computer [62]. Gradient descent iteratively updates $\boldsymbol{\theta} \rightarrow \boldsymbol{\theta} - \alpha \nabla C_{\text{train}}$ with some α until reaching a minimum after E training steps, where $\nabla C_{\text{train}}(\boldsymbol{\theta}^*) = 0$ with parameter $\boldsymbol{\theta}^*$. We assume that ansatz $U(\boldsymbol{\theta})$ can represent the target unitary V , i.e. there is a parameter $\boldsymbol{\theta}_g$ such that $C_{\text{test}}(\boldsymbol{\theta}_g, W) = C_{\text{train}}(\boldsymbol{\theta}_g, S_L) = 0$, which we enforce by choosing $V = U(\boldsymbol{\theta}_g)$ with a randomly selected $\boldsymbol{\theta}_g$.

After training we have three possible outcomes:

(i) Reach a local minimum $C_{\text{train}}(\boldsymbol{\theta}^*, S_L) > 0$,

* tobias.haug@u.nus.edu

$C_{\text{test}}(\theta^*, S_L) > 0$ with an incorrect unitary for both training set S_L and distribution W ; (ii) Reach global minimum $C_{\text{train}}(\theta^*, S_L) = 0$, however no generalization with $C_{\text{test}}(\theta^*, W) > 0$. Here, $U(\theta^*)$ correctly transform S_L , but performs poorly on states from W . (iii) Achieve global minimum and generalization with $C_{\text{train}}(\theta^*, S_L) = C_{\text{test}}(\theta^*, W) = 0$ for any state from W . In the following, we show that the DQFIM determines the critical number of circuit parameters M_c and training states L_c required to reach the global minimum and generalization which is the main result of our work.

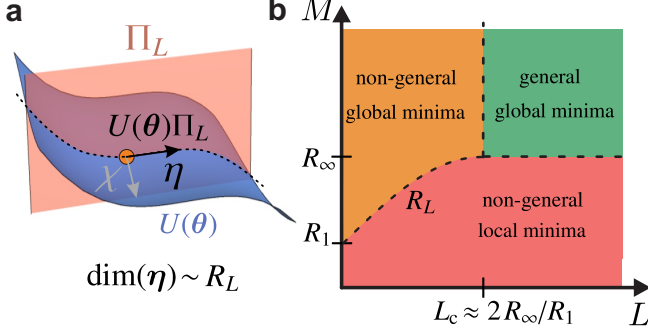


FIG. 1. **a)** We represent unitary V with ansatz unitary $U(\theta)$ by optimizing the M -dimensional parameter vector θ in respect to cost function Eq. (1) using L training states $S_L = \{|\psi_\ell\rangle, V|\psi_\ell\rangle\}_{\ell=1}^L$. Only the isometry $U(\theta)\Pi_L$ can be learned, where Π_L is the projector onto the space spanned by $\{|\psi_\ell\rangle\}_{\ell=1}^L$. The maximal rank of the data quantum Fisher information metric (DQFIM) R_L describes the degrees of freedom of $U(\theta)\Pi_L$ that can be learned with L training states. **b)** Phase diagram of optimisation and generalization with M and L . Convergence to global minimum ($C_{\text{train}} \approx 0$) is likely when $M \geq R_L$. The trained unitary can generalize to unseen test data ($C_{\text{test}} \approx 0$) for $L \geq L_c \approx 2R_\infty/R_1$ and $M \geq R_\infty$.

DQFIM.— A given training set S_L allows us to learn a part of the unitary $U(\theta)$, which we define as follows:

Definition 1 (Learnable isometry). *Given training set $S_L = \{|\psi_\ell\rangle, V|\psi_\ell\rangle\}_{\ell=1}^L$ of L states, we define projector Π_L onto the space spanned by the states $\{|\psi_\ell\rangle\}_{\ell=1}^L$ and its normalization $\tilde{\Pi}_L$*

$$\Pi_L = \sum_{k=1}^{B_L} |\phi_k\rangle\langle\phi_k|; \quad \tilde{\Pi}_L = \Pi_L/B_L \quad (3)$$

where $|\phi_k\rangle$ are the eigenvectors with non-zero eigenvalue of $\rho_L = L^{-1} \sum_{\ell=1}^L |\psi_\ell\rangle\langle\psi_\ell|$ and $B_L = \text{rank}(\rho_L)$. Training with cost function Eq. (1) learns the projection of the unitary $U(\theta)$ onto Π_L , which is the isometry

$$U_L(\theta) = U(\theta)\Pi_L. \quad (4)$$

To understand Eq. (4), let us consider the d -dimensional unitary $U \equiv U(\mathbf{u}) = \sum_{n,k=1}^d u_{nk}|n\rangle\langle k|$ with complex parameters $\mathbf{u} = \{u_{11}, u_{12}, \dots, u_{dd}\}$ and training set $S_L = \{|\ell\rangle, V|\ell\rangle\}_{\ell=1}^L$, where $|\ell\rangle \in W_{\text{comp}}$ are computational basis states and V some unitary. For $L = 1$,

training with Eq. (1) optimizes $U|1\rangle = \sum_{n=1}^d u_{n1}|n\rangle$. Here, only the parameters of the column vector $u_1 = (u_{11}, u_{21}, \dots, u_{d1})$ of U have an effect on the state and can be learned, while all other parameters are hidden. For any L , applying U on the states of S_L gives us $\{U|\ell\rangle = \sum_{n=1}^d u_{n\ell}|n\rangle\}_{\ell=1}^L$. The learnable parameters of U correspond to the $d \times L$ -dimensional isometry $U_L = (u_1, \dots, u_L) \equiv U\Pi_L$ with projector $\Pi_L = \sum_{\ell=1}^L |\ell\rangle\langle\ell|$ and $U_L^\dagger U_L = \Pi_L$ (see Fig. 1a). Even if we find a global minima with $C_{\text{train}} = 0$, training set S_L with $L < d$ provides no information about the column vectors (u_{L+1}, \dots, u_d) . The trained model $U(\mathbf{u}^*)$ will randomly guess these column vectors, resulting in generalization error $C_{\text{test}} > 0$. Only for $L = d$, we have a complete training set that can achieve generalization $C_{\text{test}} = 0$.

We can understand generalization with the number of independent parameters (or effective dimension) D_L of the isometry U_L . For $L = 1$, $U|1\rangle = \sum_{n=1}^d u_{n1}|n\rangle = \sum_{n=1}^d (a_{n1} + ib_{n1})|n\rangle$ has $2d$ real parameters a_{n1} , b_{n1} . However, due to global phase and norm, there are only $D_1 = 2d - 2$ independent parameters. For $L = d$, parameterizing a complete unitary U requires $D_d = d^2 - 1$ parameters. For example, a single qubit has $D_1 = 2$ (Bloch sphere) and $D_2 = 3$ (arbitrary unitary) free parameters [63], and thus we require $L \geq 2$ states to generalize. However, depending on ansatz and data there can be less independent parameters D_L . Let us consider $U(\theta_1, \theta_2) = \exp(-i\sigma_z\theta_1)\exp(-i\sigma_z\theta_2)$ and distribution $\{|+\rangle, |-\rangle\}$ with $|+\rangle = \frac{1}{\sqrt{2}}(|0\rangle \pm |1\rangle)$ and z -Pauli σ_z . While we have $M = 2$ parameters, the generators commute and there is only $D_1 = D_d = 1$ independent parameter and $L = 1$ state is already sufficient to generalize. In contrast, for distribution $\{|0\rangle, |1\rangle\}$ we have $D_L = 0$ and $L = 0$ as only the global phase is rotated.

For general S_L and $U(\theta)$, we now propose the DQFIM to quantify the effective dimension that can be learned (see Supplemental materials (SM) E for derivation):

Definition 2 (DQFIM). *For unitary $U(\theta)$ and training set S_L , the DQFIM is defined as*

$$\mathcal{Q}_{nm}(S_L, U(\theta)) = 4\text{Re}(\text{tr}(\partial_n U^\dagger \tilde{\Pi}_L \partial_m U) - \text{tr}(\partial_n U^\dagger \tilde{\Pi}_L U) \text{tr}(U^\dagger \tilde{\Pi}_L \partial_m U)) \quad (5)$$

where ∂_n is the derivative in respect to the n th entry of the M -dimensional vector $\theta = (\theta_1, \dots, \theta_M)$ and $\tilde{\Pi}_L$ is given by Eq. (3). We also define the effective dimension

$$D_L(S_L, U(\theta)) = \text{rank}(\mathcal{Q}(S_L, U(\theta))) \leq M. \quad (6)$$

Intuitively, $\mathcal{Q}(S_L, U(\theta))$ is a metric that describes how a variation in θ changes the isometry $U(\theta)\Pi_L$. For $L = 1$, we recover the QFIM $\mathcal{F}_{nm} = 4\text{Re}(\langle\partial_n\psi|\partial_m\psi\rangle - \langle\partial_n\psi|\psi\rangle\langle\psi|\partial_m\psi\rangle)$ [57, 64], where D_1 describes the effective dimension that a parameterized state $U(\theta)|\psi_1\rangle$ can explore [48]. D_1 increases when adding more layers G and thus parameters M to $U(\theta)$, until reaching a maximal value R_1 (see Fig. 2a). Here, the state $U(\theta)|\psi_1\rangle$ is

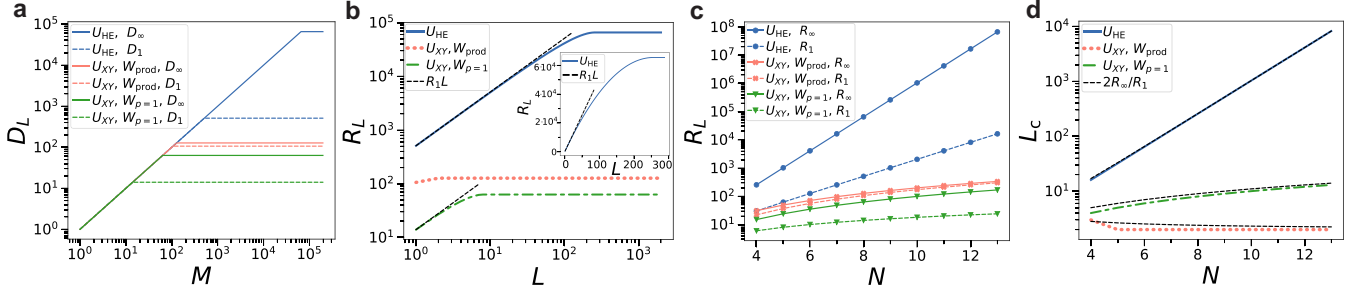


FIG. 2. DQFIM for different unitaries U with M parameters and L training states. As defined in SM A, we show hardware efficient circuit U_{HE} with no symmetries and Haar random training states (blue curves), as well as U_{XY} with particle number symmetry using as training data either product states W_{prod} (orange) or symmetry-conserving states $W_{p=1}$ (green). **a)** Effective dimension D_L increases linearly with M , until it reaches a maximal value R_L for $M \geq M_c(L)$. We have $N = 8$ qubits. **b)** R_L increases with L until converging to R_∞ for $L \geq L_c$. Black dashed line shows approximation $R_L \sim R_1 L$. Inset shows generic ansatz without log-plot, highlighting the non-linear behavior of R_L . **c)** Scaling of R_1 and R_∞ with qubit number N . **d)** Number L_c of training states needed for generalization. Black dashed line shows $L_c \approx 2R_\infty/R_1$.

overparameterized as it can explore all possible degrees of freedom of the ansatz for $L = 1$ [37]. Similarly, we introduce R_L to describe the maximal number of degrees of freedom that the isometry U_L can explore for any L :

Definition 3 (Overparameterization). *Ansatz $U(\theta, M)$ with training set S_L is overparameterized when effective dimension D_L does not increase further upon increasing the number of parameters M . The maximal rank R_L reached for $M \geq M_c(L)$ is given by*

$$R_L \equiv \max_{M \geq M_c(L), \theta} D_L(S_L, U(\theta, M)). \quad (7)$$

Once $M \geq M_c(L)$, a variation of θ can explore all degrees of freedom of U_L . Thus, minimization is unlikely to get stuck in a local minimum of cost function C_{train} [32, 37, 38, 65, 66].

Observation 1 (Convergence to global minima). *Global minimum $C_{\text{train}}(\theta^*) \approx 0$ with training set S_L is reached with high probability when $M \geq M_c(L) \geq R_L$.*

As seen in Fig. 2b, R_L and thus the circuit parameters needed to reach the global minimum increases with L , where the growth slows down due to unitary constraints. We find the upper bound (SM F or [69])

$$R_L \leq 2dL - L^2 - 1 \text{ for } L \leq d; \quad R_L \leq d^2 - 1 \text{ for } L > d. \quad (8)$$

Once the maximal possible R_L is reached, the training states are sufficient to learn all degrees of freedom of U . Thus, we have an overcomplete training set:

Definition 4 (Overcomplete data for learning unitaries). *For a given ansatz U , training set S_L of L training states $|\psi_\ell\rangle \in W$ drawn from ensemble W is overcomplete when R_L does not increase further upon increase of L . The maximal rank R_∞ is reached for L_c training states*

$$R_\infty = R_{L_c}(W, U) \equiv \max_{L \geq L_c} \mathbb{E}_{|\psi_\ell\rangle \in W} [R_L(S_L, U)]. \quad (9)$$

We bound R_L similar to R_1 for Ref. [37] (see SM G):

Theorem 1. *The maximal rank R_L is bounded by the dimension of the dynamical Lie algebra (DLA)*

$$R_L \leq \dim(\mathfrak{g}), \quad (10)$$

where $\mathfrak{g} = \text{span} \langle iH_1, \dots, iH_K \rangle_{\text{Lie}}$ is generated by the repeated nested commutators of the generators H_k of $U(\theta)$.

By choosing the training states on the support of the DLA, we can find an overcomplete training set with $L_c \leq \dim(\mathfrak{g})$. In particular, when $\dim(\mathfrak{g}) \sim \text{poly}(N)$ we have $L_c \sim \text{poly}(N)$ and $M_c \sim \text{poly}(N)$.

We can estimate L_c with the following consideration: To generalize we have to learn all R_∞ degrees of freedom of the unitary. The first training state allows us to learn R_1 degrees of freedom, while each additional state provides a bit less as seen in Eq. (8). For the upper bound Eq. (8) we have $L_c \approx 2R_\infty/R_1$, which we numerically find to be a good estimation also for other models:

Observation 2 (Generalization for learning unitaries). *A trained model generalizes $C_{\text{test}}(\theta^*) \approx 0$ with high probability when the model is overparameterized (i.e. $M \geq M_c \geq R_L$ for Def. 3) and overcomplete (i.e. $L \geq L_c$ for Def. 4). The critical number of training states L_c needed to generalize can be approximated by*

$$L_c \approx 2R_\infty/R_1. \quad (11)$$

Applications.— We want to learn the unitary evolution $V_{XY} = \exp(-iH_{XY}t)$ in time t of the XY-Hamiltonian $H_{XY} = \sum_{k=1}^N (\sigma_k^x \sigma_{k+1}^x + \sigma_k^y \sigma_{k+1}^y + h_k \sigma_k^z)$, where σ_k^α , $\alpha \in \{x, y, z\}$ is the Pauli operator acting on qubit k and $h_k \in \mathbb{R}$. We learn V_{XY} with the $U_{XY}(\theta)$ ansatz (see SM A), which can represent V_{XY} with a polynomially number of parameters [70]. Further, H_{XY} and U_{XY} are symmetric in respect to the particle number operator $P = \sum_{k=1}^N \frac{1}{2}(1 + \sigma_k^z)$ with $[U_{XY}, P] = [H_{XY}, P] = 0$, where $[\cdot]$ is the commutator. We define the distribution

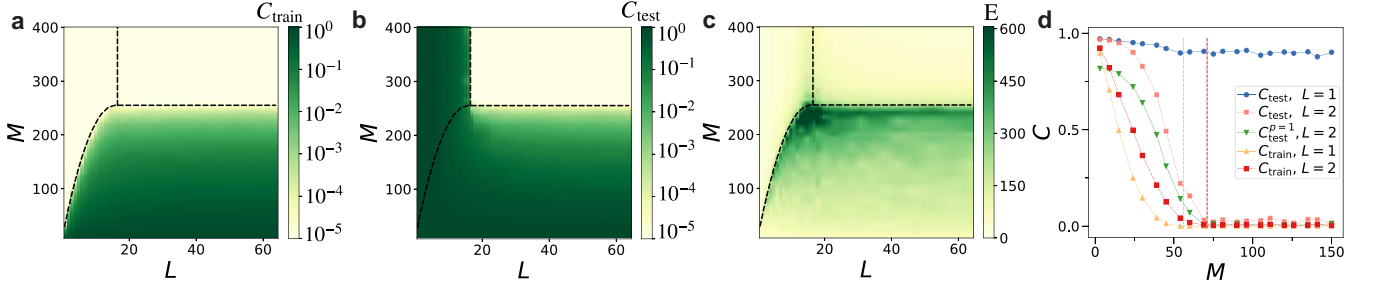


FIG. 3. **a)** C_{train} against M and L . Dashed black lines indicate $M_c(L) = R_L$ and $L_c = 2R_\infty/R_1$. We have a $N = 4$ qubit hardware-efficient ansatz with Haar random training states, where we initialize with a random parameter, train with a gradient descent algorithm [67] simulated with [68] and average over 10 training repetitions. Target unitary is chosen as $V = U(\theta_g)$, where θ_g is a random parameter of the ansatz unitary. **b)** Average C_{test} against M and L . **c)** Number of training steps E until reaching $C_{\text{train}} < 10^{-4}$. **d)** C_{test} and C_{train} against M with U_{XY} ansatz for $N = 6$ qubits, where we train with $L = 1$ and $L = 2$ product states W_{prod} . We use W_{prod} as test states, except for green dotted curve $C_{\text{test}}^{p=1}$ where we show out-of-distribution generalization with symmetric test states $W_{p=1}$. The dashed vertical lines indicate R_1 (yellow) and R_2 (red).

$W_{p=1}$ of states $|\psi_\ell\rangle$ which are symmetric in regards to P , i.e. $P|\psi_\ell\rangle = |\psi_\ell\rangle$ with the same eigenvalue $p = 1$ for all ℓ . Further, we define the distribution of single-qubit product states W_{prod} where $|\psi_\ell\rangle = \bigotimes_{k=1}^N |\phi_\ell^k\rangle$, $|\phi_\ell^k\rangle \in \mathcal{H}(\mathbb{C}^2)$ which do not respect particle symmetry in general. We now study generalization with U_{XY} depending on the symmetry of the training states:

Observation 3 (Generalization requires more data with symmetries). *Ansatz U_{XY} conserves particle number operator P with $[U_{XY}, P] = 0$. We learn with (i) the ensemble of particle-number conserving states $|\psi_\ell\rangle \in W_{p=1}$ and (ii) single-qubit product states $|\psi_\ell\rangle \in W_{\text{prod}}$. We generalize with $L \geq L_c$ training states where*

- (i) $L_c = N$ for $|\psi_\ell\rangle \in W_{p=1}$
- (ii) $L_c = 2$ for $|\psi_\ell\rangle \in W_{\text{prod}}$, $N > 4$.

This result follows directly from the scaling of R_L (see Fig. 2c,d). In particular, for $W_{p=1}$ we have $R_1 = 2N - 2$, $R_\infty = N^2 - 1$, while for W_{prod} we find via numerical extrapolation $R_1 = 2N^2 - 3N + 2$ and $R_\infty = 2N^2 - 1$. Generalization improves without symmetries as R_1 grows larger for $p > 1$ and thus product states with support on all p gain more information about U_{XY} than data restricted to $p = 1$.

Next, we consider out-of-distribution generalization where one generates the training set from a different ensemble than the test states [8]:

Observation 4 (Out-of-distribution generalization requires less data). *Training U_{XY} with $L \geq 2$ product states $|\psi_\ell\rangle \in W_{\text{prod}}$ out-of-distribution generalizes symmetry conserving data $W_{p=1}$ with $C_{\text{test}}(\theta^*, W_{\text{prod}}) = C_{\text{test}}(\theta^*, W_{p=1}) = 0$. In contrast, training U_{XY} with $|\psi_\ell\rangle \in W_{p=1}$ requires $L \geq N$ training states to achieve $C_{\text{test}}(\theta^*, W_{p=1}) = 0$.*

Numerical results.— In Fig. 3a-c we study training for hardware-efficient ansatz U_{HE} (see SM A). In Fig. 3a, we converge to local minima with $C_{\text{train}} \gg 0$ for $M \leq R_L$,

while we find global minimum $C_{\text{train}} \approx 0$ for $M \geq R_L$, which is indicated as black dashed line. In Fig. 3b, generalization $C_{\text{test}} \approx 0$ is achieved only for $M \geq R_\infty$ and $L \geq L_c \approx 2R_\infty/R_1$ indicated by the vertical black lines. In Fig. 3c, the number of training steps E needed to converge show characteristic peaks close to M_c and L_c indicated by black dashed lines. In Fig. 3d we study test and training error for the U_{XY} ansatz for training with product state ensemble W_{prod} . For sufficient M , we have $C_{\text{train}} \approx 0$ for $L = 1$ and $L = 2$ training data. Generalization with $C_{\text{test}} \approx 0$ requires $L \geq 2$ when testing in-distribution W_{prod} or out-of-distribution $W_{p=1}$. We study other models which generalize for constant L in SM J and I.

In Fig. 4a we study C_{test} against L , M for U_{XY} when training with particle-conserved ensemble $W_{p=1}$ (see also SM C). Generalization improves with M and L , where the lower bound $C_{\text{test}} \sim 1 - (L/L_c)^2$ [6] is saturated for $M \geq M_c$. In Fig. 4b, we show that the training steps needed for convergence scale as $E \sim N^2$ with a clear peak at $L \approx L_c$ when overparameterized.

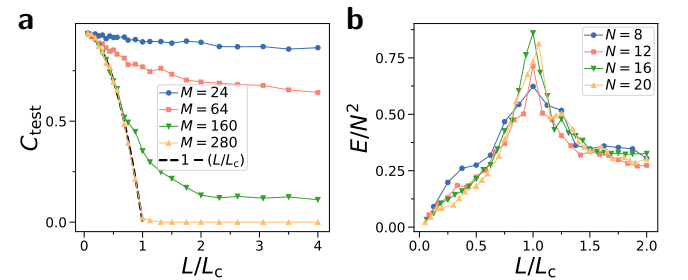


FIG. 4. Learning with U_{XY} and particle conserved data $|\psi_\ell\rangle \in W_{p=1}$. **a)** C_{test} against L for different M with $N = 16$, $L_c = N$. Black dashed line is $C_{\text{test}} \sim 1 - (L/L_c)^2$. **b)** Training steps E needed to converge to $C_{\text{train}} < 10^{-4}$ against L for $M \gg M_c$.

Conclusion.— The newly introduced DQFIM \mathcal{Q} and its maximal rank R_L tell us the amount of data L

and circuit parameters M needed to successfully learn unitaries. Overparameterized models [32, 37, 38] converge to a global minimum with high probability for $M \geq M_c \geq R_L$. Generalization, i.e. correctly predicting new data, requires a critical number of training states $L \geq L_c$, which depends on the ratio $L_c \approx 2R_\infty/R_1$. Overparameterization and generalization appear in three distinct regimes, where training time increases substantially at the transitions, which could indicate a computational phase transition [24, 32]. While the complexity of unitaries grows linearly with M [48, 71], the growth in learnable degrees of freedom R_L and thus the circuit depth needed for overparameterization slows down with L . Generalization for overparameterized models scales as $C_{\text{test}} \sim 1 - (L/L_c)^2$ saturating the lower bound of Ref. [6], which is substantially better than the upper bound $C_{\text{test}} \sim \sqrt{1/L}$ [7, 59]. For underparameterized models the empirical risk $C_{\text{test}} - C_{\text{train}}$ [59] can insufficiently characterize generalization due to convergence to bad local minima (see SM B).

We show that generalization and overparameterization can be achieved with polynomial circuit depth and dataset size when the dimension of the DLA scales polynomially with N . When $R_1 \sim N^\gamma$, $R_\infty \sim N^\gamma$ scale with the same γ , then $O(1)$ training states are sufficient

to generalize, explaining the numerical observations of Ref. [10] (see also SM I). While symmetries can improve generalization [44, 45], we show that symmetries in data can also hinder generalization by increasing the R_∞/R_1 ratio. Generalization improves here as symmetry-broken data has access to information of other symmetry sectors. This feature also allows out-of-distribution generalization [8] to outperform in-distribution generalization. Note that symmetry-broken data requires slightly more parameters, which implies an interesting trade-off between dataset size and circuit depth. Finally, the DQFIM could be extended to evaluate generalization for other quantum machine learning tasks [20] as well as data re-uploading [72, 73], kernel models [74, 75] and the effect of noise [58]. The code for this work is available online [76].

ACKNOWLEDGMENTS

Acknowledgements— We acknowledge discussions with Adithya Sireesh. This work is supported by a Samsung GRC project and the UK Hub in Quantum Computing and Simulation, part of the UK National Quantum Technologies Programme with funding from UKRI EPSRC grant EP/T001062/1.

-
- [1] J. Biamonte, P. Wittek, N. Pancotti, P. Rebentrost, N. Wiebe, and S. Lloyd, Quantum machine learning, *Nature* **549**, 195 (2017).
 - [2] K. Poland, K. Beer, and T. J. Osborne, No free lunch for quantum machine learning, arXiv preprint arXiv:2003.14103 (2020).
 - [3] M. C. Caro and I. Datta, Pseudo-dimension of quantum circuits, *Quantum Machine Intelligence* **2**, 14 (2020).
 - [4] A. Abbas, D. Sutter, C. Zoufal, A. Lucchi, A. Figalli, and S. Woerner, The power of quantum neural networks, *Nature Computational Science* **1**, 403 (2021).
 - [5] A. Abbas, D. Sutter, A. Figalli, and S. Woerner, Effective dimension of machine learning models, arXiv:2112.04807 (2021).
 - [6] K. Sharma, M. Cerezo, Z. Holmes, L. Cincio, A. Sornborger, and P. J. Coles, Reformulation of the no-free-lunch theorem for entangled datasets, *Physical Review Letters* **128**, 070501 (2022).
 - [7] L. Banchi, J. Pereira, and S. Pirandola, Generalization in quantum machine learning: A quantum information standpoint, *PRX Quantum* **2**, 040321 (2021).
 - [8] M. C. Caro, H.-Y. Huang, N. Ezzell, J. Gibbs, A. T. Sornborger, L. Cincio, P. J. Coles, and Z. Holmes, Out-of-distribution generalization for learning quantum dynamics, arXiv:2204.10268 (2022).
 - [9] E. Peters and M. Schuld, Generalization despite overfitting in quantum machine learning models, arXiv:2209.05523 (2022).
 - [10] J. Gibbs, Z. Holmes, M. C. Caro, N. Ezzell, H.-Y. Huang, L. Cincio, A. T. Sornborger, and P. J. Coles, Dynamical simulation via quantum machine learning with provable generalization, arXiv:2204.10269 (2022).
 - [11] T. Volkoff, Z. Holmes, and A. Sornborger, Universal compiling and (no-) free-lunch theorems for continuous-variable quantum learning, *PRX Quantum* **2**, 040327 (2021).
 - [12] H. Cai, Q. Ye, and D.-L. Deng, Sample complexity of learning parametric quantum circuits, *Quantum Science and Technology* **7**, 025014 (2022).
 - [13] C. M. Popescu, Learning bounds for quantum circuits in the agnostic setting, *Quantum Information Processing* **20**, 286 (2021).
 - [14] M. C. Caro, E. Gil-Fuster, J. J. Meyer, J. Eisert, and R. Sweke, Encoding-dependent generalization bounds for parametrized quantum circuits, *Quantum* **5**, 582 (2021).
 - [15] K. Bu, D. E. Koh, L. Li, Q. Luo, and Y. Zhang, Statistical complexity of quantum circuits, *Physical Review A* **105**, 062431 (2022).
 - [16] J. Bowles, V. J. Wright, M. Farkas, N. Killoran, and M. Schuld, Contextuality and inductive bias in quantum machine learning, arXiv:2302.01365 (2023).
 - [17] Y. Du, Y. Yang, D. Tao, and M.-H. Hsieh, Demystify problem-dependent power of quantum neural networks on multi-class classification, arXiv:2301.01597 (2022).
 - [18] A. Bisio, G. Chiribella, G. M. D'Ariano, S. Facchini, and P. Perinotti, Optimal quantum learning of a unitary transformation, *Physical Review A* **81**, 032324 (2010).
 - [19] I. Marvian and S. Lloyd, Universal quantum emulator, arXiv preprint arXiv:1606.02734 (2016).
 - [20] K. Bharti, A. Cervera-Lierta, T. H. Kyaw, T. Haug, S. Alperin-Lea, A. Anand, M. Degroote, H. Heimonen, J. S. Kottmann, T. Menke, W.-K. Mok, S. Sim, L.-C.

- Kwek, and A. Aspuru-Guzik, Noisy intermediate-scale quantum algorithms, *Rev. Mod. Phys.* **94**, 015004 (2022).
- [21] M. Cerezo, A. Arrasmith, R. Babbush, S. C. Benjamin, S. Endo, K. Fujii, J. R. McClean, K. Mitarai, X. Yuan, L. Cincio, *et al.*, Variational quantum algorithms, *Nature Reviews Physics* **3**, 625 (2021).
 - [22] S. Xue, Y. Liu, Y. Wang, P. Zhu, C. Guo, and J. Wu, Variational quantum process tomography of unitaries, *Physical Review A* **105**, 032427 (2022).
 - [23] V. Gebhart, R. Santagati, A. A. Gentile, E. M. Gauger, D. Craig, N. Ares, L. Bianchi, F. Marquardt, L. Pezzè, and C. Bonato, Learning quantum systems, *Nature Reviews Physics* , 1 (2023).
 - [24] B. T. Kiani, S. Lloyd, and R. Maity, Learning unitaries by gradient descent, *arXiv:2001.11897* (2020).
 - [25] S. Khatri, R. LaRose, A. Poremba, L. Cincio, A. T. Sornborger, and P. J. Coles, Quantum-assisted quantum compiling, *Quantum* **3**, 140 (2019).
 - [26] N. Ezzell, E. M. Ball, A. U. Siddiqui, M. M. Wilde, A. T. Sornborger, P. J. Coles, and Z. Holmes, Quantum mixed state compiling, *arXiv:2209.00528* (2022).
 - [27] C. Cirstoiu, Z. Holmes, J. Iosue, L. Cincio, P. J. Coles, and A. Sornborger, Variational fast forwarding for quantum simulation beyond the coherence time, *npj Quantum Information* **6**, 82 (2020).
 - [28] J. Gibbs, K. Gili, Z. Holmes, B. Commeau, A. Arrasmith, L. Cincio, P. J. Coles, and A. Sornborger, Long-time simulations for fixed input states on quantum hardware, *npj Quantum Information* **8**, 135 (2022).
 - [29] J. Romero, J. P. Olson, and A. Aspuru-Guzik, Quantum autoencoders for efficient compression of quantum data, *Quantum Sci. Technol.* **2**, 045001 (2017).
 - [30] H. Zhang, L. Wan, T. Haug, W.-K. Mok, S. Paesani, Y. Shi, H. Cai, L. K. Chin, M. F. Karim, L. Xiao, *et al.*, Resource-efficient high-dimensional subspace teleportation with a quantum autoencoder, *Science Advances* **8**, eabn9783 (2022).
 - [31] L. Leone, S. F. Oliviero, S. Piemontese, S. True, and A. Hama, Retrieving information from a black hole using quantum machine learning, *Physical Review A* **106**, 062434 (2022).
 - [32] E. R. Anschuetz, Critical points in quantum generative models, *arXiv:2109.06957* (2021).
 - [33] E. R. Anschuetz and B. T. Kiani, Quantum variational algorithms are swamped with traps, *Nature Communications* **13**, 7760 (2022).
 - [34] L. Bittel and M. Kliesch, Training variational quantum algorithms is np-hard, *Physical review letters* **127**, 120502 (2021).
 - [35] X. You and X. Wu, Exponentially many local minima in quantum neural networks, in *International Conference on Machine Learning* (PMLR, 2021) pp. 12144–12155.
 - [36] J. R. McClean, S. Boixo, V. N. Smelyanskiy, R. Babbush, and H. Neven, Barren plateaus in quantum neural network training landscapes, *Nature communications* **9**, 4812 (2018).
 - [37] M. Larocca, N. Ju, D. García-Martín, P. J. Coles, and M. Cerezo, Theory of overparametrization in quantum neural networks, *arXiv:2109.11676* (2021).
 - [38] X. You, S. Chakrabarti, and X. Wu, A convergence theory for over-parameterized variational quantum eigensolvers, *arXiv:2205.12481* (2022).
 - [39] R. Wiersema, C. Zhou, Y. de Sereville, J. F. Carrasquilla, Y. B. Kim, and H. Yuen, Exploring entanglement and optimization within the hamiltonian variational ansatz, *PRX Quantum* **1**, 020319 (2020).
 - [40] L. Schatzki, M. Larocca, F. Sauvage, and M. Cerezo, Theoretical guarantees for permutation-equivariant quantum neural networks, *arXiv:2210.09974* (2022).
 - [41] M. Ragone, P. Braccia, Q. T. Nguyen, L. Schatzki, P. J. Coles, F. Sauvage, M. Larocca, and M. Cerezo, Representation theory for geometric quantum machine learning, *arXiv:2210.07980* (2022).
 - [42] Q. T. Nguyen, L. Schatzki, P. Braccia, M. Ragone, P. J. Coles, F. Sauvage, M. Larocca, and M. Cerezo, Theory for equivariant quantum neural networks, *arXiv:2210.08566* (2022).
 - [43] H. Zheng, Z. Li, J. Liu, S. Strelchuk, and R. Kondor, Speeding up learning quantum states through group equivariant convolutional quantum ansätze, *arXiv:2112.07611* (2021).
 - [44] J. J. Meyer, M. Mularski, E. Gil-Fuster, A. A. Mele, F. Arzani, A. Wilms, and J. Eisert, Exploiting symmetry in variational quantum machine learning, *PRX Quantum* **4**, 010328 (2023).
 - [45] M. Larocca, F. Sauvage, F. M. Sbahi, G. Verdon, P. J. Coles, and M. Cerezo, Group-invariant quantum machine learning, *PRX Quantum* **3**, 030341 (2022).
 - [46] F. Sauvage, M. Larocca, P. J. Coles, and M. Cerezo, Building spatial symmetries into parameterized quantum circuits for faster training, *arXiv:2207.14413* (2022).
 - [47] A. Skolik, M. Cattelan, S. Yarkoni, T. Bäck, and V. Dunjko, Equivariant quantum circuits for learning on weighted graphs, *arXiv preprint arXiv:2205.06109* (2022).
 - [48] T. Haug, K. Bharti, and M. Kim, Capacity and quantum geometry of parametrized quantum circuits, *PRX Quantum* **2**, 040309 (2021).
 - [49] E. R. Anschuetz, A. Bauer, B. T. Kiani, and S. Lloyd, Efficient classical algorithms for simulating symmetric quantum systems, *arXiv preprint arXiv:2211.16998* (2022).
 - [50] H.-Y. Huang, M. Broughton, M. Mohseni, R. Babbush, S. Boixo, H. Neven, and J. R. McClean, Power of data in quantum machine learning, *Nature communications* **12**, 1 (2021).
 - [51] Y. Liu, S. Arunachalam, and K. Temme, A rigorous and robust quantum speed-up in supervised machine learning, *Nature Physics* , 1 (2021).
 - [52] H.-Y. Huang, R. Kueng, G. Torlai, V. V. Albert, and J. Preskill, Provably efficient machine learning for quantum many-body problems, *Science* **377**, eabk3333 (2022).
 - [53] J. Liu, M. Liu, J.-P. Liu, Z. Ye, Y. Alexeev, J. Eisert, and L. Jiang, Towards provably efficient quantum algorithms for large-scale machine-learning models, *arXiv:2303.03428* (2023).
 - [54] P. L. Bartlett, D. J. Foster, and M. J. Telgarsky, Spectrally-normalized margin bounds for neural networks, *Advances in neural information processing systems* **30** (2017).
 - [55] Y. Jiang, B. Neyshabur, H. Mobahi, D. Krishnan, and S. Bengio, Fantastic generalization measures and where to find them, *arXiv:1912.02178* (2019).
 - [56] T. Liang, T. Poggio, A. Rakhlin, and J. Stokes, Fisher-rao metric, geometry, and complexity of neural networks, in *The 22nd international conference on artificial intelligence and statistics* (PMLR, 2019) pp. 888–896.
 - [57] J. J. Meyer, Fisher information in noisy intermediate-

- scale quantum applications, *Quantum* **5**, 539 (2021).
- [58] D. García-Martín, M. Larocca, and M. Cerezo, Effects of noise on the overparametrization of quantum neural networks, arXiv:2302.05059 (2023).
 - [59] M. C. Caro, H.-Y. Huang, M. Cerezo, K. Sharma, A. Sornborger, L. Cincio, and P. J. Coles, Generalization in quantum machine learning from few training data, *Nature communications* **13**, 4919 (2022).
 - [60] J. C. Garcia-Escartin and P. Chamorro-Posada, Swap test and hong-ou-mandel effect are equivalent, *Physical Review A* **87**, 052330 (2013).
 - [61] R. Chakrabarti and H. Rabitz, Quantum control landscapes, *International Reviews in Physical Chemistry* **26**, 671 (2007).
 - [62] K. Mitarai, M. Negoro, M. Kitagawa, and K. Fujii, Quantum circuit learning, *Physical Review A* **98**, 032309 (2018).
 - [63] M. A. Nielsen and I. Chuang, *Quantum computation and quantum information* (2002).
 - [64] J. Liu, H. Yuan, X.-M. Lu, and X. Wang, Quantum fisher information matrix and multiparameter estimation, *Journal of Physics A: Mathematical and Theoretical* **53**, 023001 (2020).
 - [65] H. A. Rabitz, M. M. Hsieh, and C. M. Rosenthal, Quantum optimally controlled transition landscapes, *Science* **303**, 1998 (2004).
 - [66] M. Bukov, A. G. R. Day, D. Sels, P. Weinberg, A. Polkovnikov, and P. Mehta, Reinforcement learning in different phases of quantum control, *Phys. Rev. X* **8**, 031086 (2018).
 - [67] R. Fletcher, *Practical methods of optimization* (John Wiley & Sons, 2013).
 - [68] J. R. Johansson, P. D. Nation, and F. Nori, Qutip: An open-source python framework for the dynamics of open quantum systems, *Computer Physics Communications* **183**, 1760 (2012).
 - [69] J. Polcarí, *Representing unitary matrices by independent parameters*, Tech. Rep. (Working Paper, Rev 0, October, 2016, 2016).
 - [70] E. Kökcü, D. Camps, L. B. Otfelie, J. K. Freericks, W. A. de Jong, R. Van Beeumen, and A. F. Kemper, Algebraic compression of quantum circuits for hamiltonian evolution, *Physical Review A* **105**, 032420 (2022).
 - [71] J. Haferkamp, P. Faist, N. B. Kothakonda, J. Eisert, and N. Yunger Halpern, Linear growth of quantum circuit complexity, *Nature Physics* **18**, 528 (2022).
 - [72] A. Pérez-Salinas, A. Cervera-Liarta, E. Gil-Fuster, and J. I. Latorre, Data re-uploading for a universal quantum classifier, *Quantum* **4**, 226 (2020).
 - [73] S. Jerbi, L. J. Fiderer, H. Poulsen Nautrup, J. M. Kübler, H. J. Briegel, and V. Dunjko, Quantum machine learning beyond kernel methods, *Nature Communications* **14**, 517 (2023).
 - [74] M. Schuld and N. Killoran, Quantum machine learning in feature hilbert spaces, *Physical review letters* **122**, 040504 (2019).
 - [75] T. Haug, C. N. Self, and M. S. Kim, Quantum machine learning of large datasets using randomized measurements, *Machine Learning: Science and Technology* **4**, 015005 (2023).
 - [76] T. Haug, Generalization with quantum geometry, https://github.com/txhaug/geometric_generalization.
 - [77] R. Cheng, Quantum geometric tensor (fubini-study metric) in simple quantum system: A pedagogical introduction, arXiv:1012.1337 (2010).
 - [78] D. d'Alessandro, *Introduction to quantum control and dynamics* (Chapman and hall/CRC, 2021).

CONTENTS

A.	Ansatz unitaries	8
B.	Generalization and empirical risk	9
C.	Training of XY model	9
D.	Quantum Fisher information metric	10
E.	Data quantum Fisher information metric	12
F.	Degrees of freedom of isometries	13
G.	Lie-algebra bounds DQFIM	13
H.	Ansatz unitaries for SM	15
I.	Generalization with further models	15
J.	Training of Y-CZ model	16

Appendix A: Ansatz unitaries

The ansatz unitaries used in the main text are shown in Fig. 5. We assume that the considered unitaries have a periodic structure of G layers with

$$U(\boldsymbol{\theta}) = \prod_{k=1}^G U_k(\boldsymbol{\theta}_k), \quad U^{(k)}(\boldsymbol{\theta}_k) = \prod_{n=1}^K \exp(-i\theta_{kn} H_n) \quad (\text{A1})$$

where $U^{(k)}(\boldsymbol{\theta}_k)$ is the unitary of the k th layer. Here, H_n are K hermitian matrices and $\boldsymbol{\theta}_k = \{\theta_{k1}, \dots, \theta_{kn}\}$ are the parameters of the k th layer. The total parameter vector $\boldsymbol{\theta} = \{\boldsymbol{\theta}_1, \dots, \boldsymbol{\theta}_G\}$ of the ansatz has $M = GK$ parameters.

In Fig. 5a, we show a hardware efficient ansatz U_{HE} , which produces highly random circuits which span the full Hilbertspace nearly uniformly and are known to be hard to simulate classically. Overparameterization requires for this circuit exponentially many parameters.

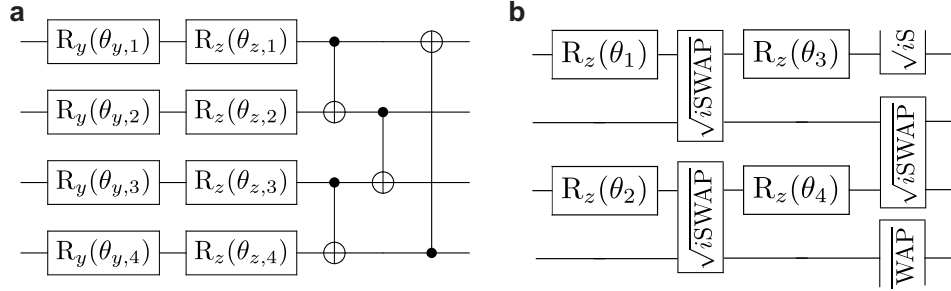


FIG. 5. Ansatz unitaries for the main text. The circuits are repeated for G layers. **a)** Hardware-efficient ansatz U_{HE} consisting of parameterized y, z rotations and CNOT gates. Has no symmetries and can realize arbitrary N -qubit unitaries for sufficient depth. **b)** U_{XY} circuit inspired by XY-model Eq. (A2). Composed of single qubit z rotations and nearest-neighbor $\sqrt{i}\text{SWAP}$ gates, arranged with periodic boundary condition. Commutes with particle number operator P and for sufficient depth can realize any time evolution generated by $\exp(-iH_{XY}t)$. **c)** Real-valued ansatz $U_{Y\text{-CZ}}$ consisting of y -rotations and control- Z gates in a nearest-neighbor chain configuration.

In Fig. 5b, we show an ansatz U_{XY} with symmetries that overparameterizes in polynomial depth. This ansatz is inspired from the integrable XY Hamiltonian with random field h_k

$$H_{XY} = \sum_{k=1}^N h_k \sigma_k^z + \sum_{k=1}^N (\sigma_k^x \sigma_{k+1}^x + \sigma_k^y \sigma_{k+1}^y) \quad (\text{A2})$$

H_{XY} commutes with the particle number operator $P = \sum_{k=1}^N \frac{1}{2}(1 + \sigma_k^z)$ where σ_k^z is the Pauli z operator acting on qubit k . In particular, we have $[H_{XY}, P]$. Time evolution $U = \exp(-iH_{XY}t)$ also conserves the symmetry, i.e. $[U, P] = 0$. The ansatz U_{XY} shown in 5b can represent the time evolution of the Hamiltonian. U_{XY} consists of parameterized z -rotations and nearest-neighbor $\sqrt{\text{iSWAP}} = \exp(i\pi/8(\sigma_k^x \sigma_{k+1}^x + \sigma_k^y \sigma_{k+1}^y))$ gates. One can think of this model similar to a Trotterized version of the time evolution $U = \exp(-iH_{XY}t)$. The generators of U_{XY} are the Pauli operators of H_{XY} . Thus, the time-evolution operator U_{XY} spans the same dynamical Lie algebra as the time evolution generated by H_{XY} and can represent any time evolution of H_{XY} [70]. The dimension of the dynamical Lie-algebra spanned by U_{XY} scales polynomial with qubit number N and thus can be overparameterized with polynomially many parameters M [37]. For random product states W_{prod} as training set, we find via numerical extrapolation $R_1 = 2N^2 - 3N + 2$ and $R_\infty = 2N^2 - 1$. We also choose a training set $W_{p=1}$ with $P = 1$ particles, which consists of arbitrary superpositions of permutations of the basis states $|10\dots 0\rangle$. We have $P|\psi_\ell\rangle = |\psi_\ell\rangle$ for any state $|\psi_\ell\rangle \in W_{p=1}$. These states live in an effective N -dimensional subspace, yielding $R_1 = 2N - 2$ and $R_\infty = N^2 - 1$.

Appendix B: Generalization and empirical risk

We define generalization via the error of the cost function C_{test} averages over the full data ensemble W . In our studies, we choose the problem such that $C_{\text{test}} = 0$ can be achieved for at least one parameter θ_g .

In general, the minimal achievable C_{test} for given ansatz and data distribution may not be known. Thus, often the empirical risk $\zeta = C_{\text{test}} - C_{\text{train}}$ of the trained model is used as a proxy to evaluate generalization [59]. In Fig. 6, we compare C_{train} , C_{test} and empirical risk $C_{\text{test}} - C_{\text{train}}$. We show the hardware-efficient ansatz with $N = 4$ overparameterizes for $M \geq M_c = 4^N - 1 = 255$ and $L_c = 2^N = 16$. When the model is underparameterized $M \leq M_c$, the training error in Fig. 6a and test error in Fig. 6b can be quite large. In contrast, the empirical risk in Fig. 6c shows favorable scaling with L . However, note that the actual test error decreases in absolute value only slightly with L . Overparameterization $M \geq M_c$ drastically reduces the training error to zero, and for $L \geq L_c$ allows us to find $C_{\text{test}} \approx 0$.

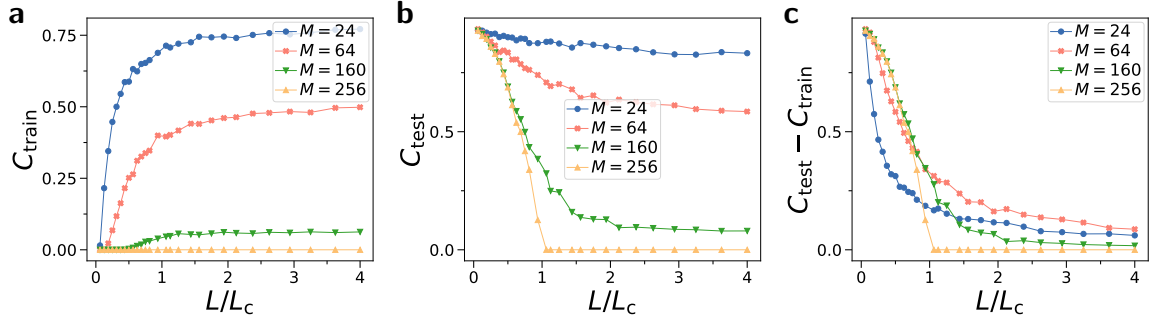


FIG. 6. Training error, test error and empirical risk for hardware-efficient ansatz with Haar random training states for $N = 4$ qubits. We assume that there is an optimal solution, i.e. there is at least one parameter with $C_{\text{test}}(\theta_g) = 0$. **a)** C_{train} against L for different M . **b)** C_{test} against L for different M . **c)** Empirical risk $C_{\text{test}} - C_{\text{train}}$ against L for different M .

In Fig. 7 we study generalization and empirical risk for U_{XY} ansatz and symmetric data $W_{p=1}$. In Fig. 7a,b we see that C_{train} and C_{test} decreases with M , and reaches near-zero for $M \geq M_c$. In Fig. 7c we plot the empirical risk $C_{\text{test}} - C_{\text{train}}$ against M . We find that the empirical risk first increases, then decreases with M . We also note that the empirical risk increases with N .

Appendix C: Training of XY model

We now show additional numerical results on training with the U_{XY} ansatz and symmetric data $W_{p=1}$.

In Fig. 8a, we study generalization in the overparameterized regime. We find $C_{\text{test}} \sim 1 - (L/L_c)^2$ independent of N .

In Fig. 8b we study the steps E needed to converge against M for different N for overcomplete data $L \gg L_c$. We observe $E \sim N^2$. At M_c the steps needed to converge sharply decreases, indicating the transition to an optimization landscape where the global minimum can be reached easily.

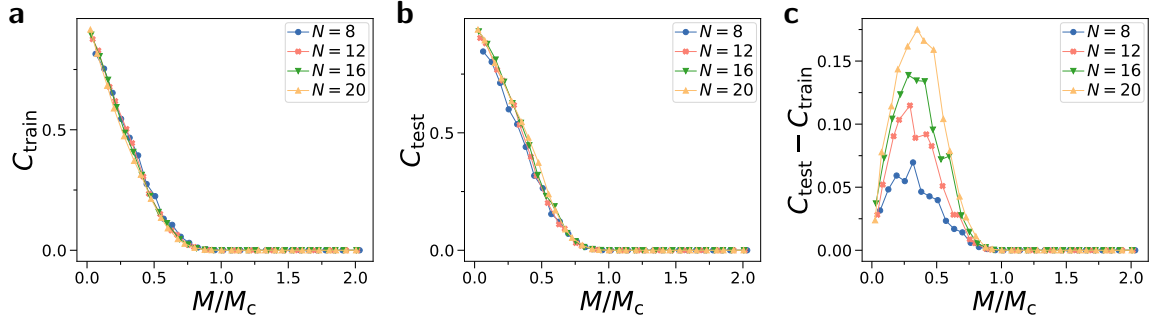


FIG. 7. Learning with U_{XY} and $|\psi_\ell\rangle \in W_{p=1}$ with fixed overcomplete data $L = 40 \gg L_c$ for $N = 16$. **a)** C_{train} against M for different N , where $M_c = N^2 - 1 = 255$. **b)** C_{test} against M for different N . **c)** Empirical risk $C_{\text{test}} - C_{\text{train}}$ against M .

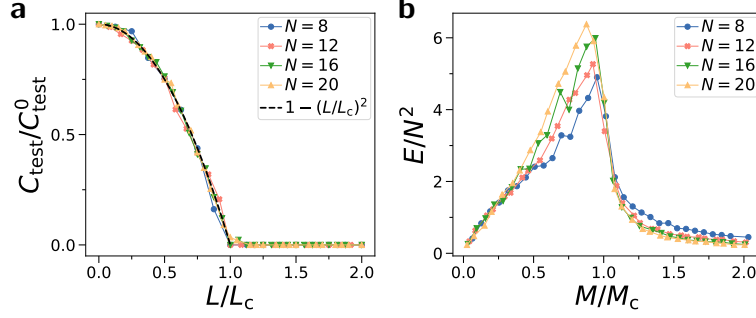


FIG. 8. Learning with U_{XY} and $|\psi_\ell\rangle \in W_{p=1}$. **a)** Test error C_{test} relative to error without training C_{test}^0 for varying training set size L and $M \gg M_c$. We find $C_{\text{test}}/C_{\text{test}}^0 = 1 - (L/L_c)^2$, where $L_c = N$ and we average over 10 random instances. **b)** Training steps E required to find $C_{\text{test}} < 10^{-3}$.

Fig. 9, we show two-dimensional plots of C_{train} , C_{test} and number of iterations E against L and M . We find training and test error matches closely the transitions derived from R_L which are shown as black dashed lines.

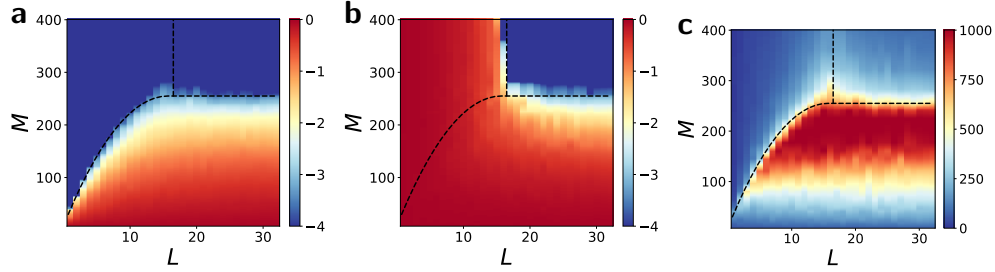


FIG. 9. Mean error for training U_{XY} for symmetric data $W_{p=1}$ for $N = 16$ qubits. **a)** C_{train} against M and L . Color shows logarithm $\log_{10}(C_{\text{train}})$. **b)** C_{test} against M and L . **c)** Number of training steps E until reaching $C_{\text{train}} < 10^{-3}$.

Next, we show the U_{XY} ansatz where we learn with random product states W_{prod} in Fig.10. Here, we generalize already for $L \geq 2$. In Fig.10d, we show out-of-distribution generalization, where we train with W_{prod} , but test with $W_{p=1}$. We find the same test error as when testing with W_{prod} .

Appendix D: Quantum Fisher information metric

The Quantum Fisher information metric (QFIM) [57, 64] is an essential tool for quantum sensing, parameter estimation and optimization of quantum circuits. Here, we review the derivation of the QFIM or Fubini-Study metric \mathcal{F} [77]. We have a parameterized quantum state $|\psi(\theta)\rangle$. We now study the variation

$$ds^2 = ||\psi(\theta + d\theta)\rangle - |\psi(\theta)\rangle|| = \langle \delta\psi | \delta\psi \rangle =$$

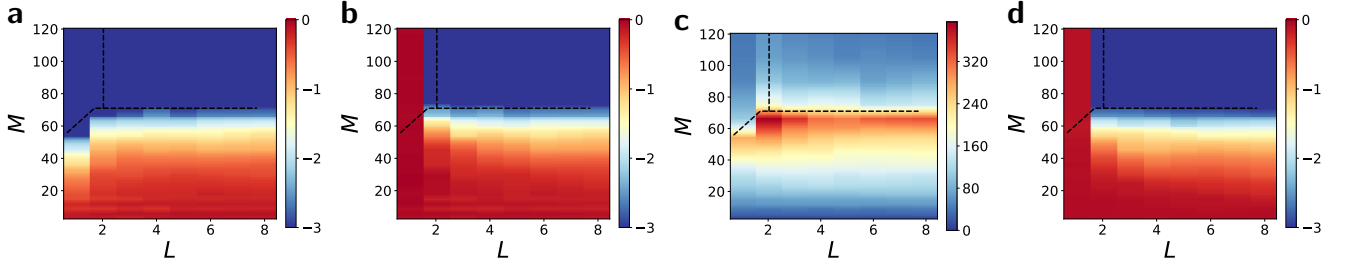


FIG. 10. Mean error for training U_{XY} ansatz for random product state data sampled from W_{prod} and $N = 6$ qubits. **a)** C_{train} against M and L . Color shows logarithm $\log_{10}(C_{\text{train}})$. **b)** C_{test} against M and L tested against W_{prod} . **c)** Number of training steps E until reaching $C_{\text{train}} < 10^{-3}$. **d)** Out-of-distribution generalization C_{test} against M and L tested against $W_{p=1}$.

$$\langle \partial_n \psi | \partial_m \psi \rangle d\theta^n d\theta^m = (\gamma_{nm} + i\sigma_{nm}) d\theta^n d\theta^m$$

where we defined the real and imaginary part γ_{nm} and σ_{nm} of $\langle \partial_n \psi | \partial_m \psi \rangle$. As ds^2 is hermitian, we have $\gamma_{nm} = \gamma_{mn}$ and $\sigma_{nm} = -\sigma_{mn}$, such that $\sigma_{nm} d\theta^n d\theta^m$ vanishes. However, γ_{nm} is not a proper metric as it is not invariant under the gauge transformation $|\psi'\rangle = \exp(i\alpha)|\psi\rangle$ under a global phase rotation with α . We now construct a proper gauge invariant metric.

First, one can easily show by using $\langle \psi | \psi \rangle = 1$ that $\beta_n = i\langle \psi | \partial_n \psi \rangle \in \mathbb{R}$. Next, we compute $\langle \psi' | \psi' \rangle = \gamma'_{nm} + i\sigma'_{nm}$, where a straightforward calculation yields

$$\gamma'_{nm} = \gamma_{nm} + \partial_n \alpha \partial_m \alpha - \beta_m \gamma_n \alpha - \beta_n \gamma_m \quad (\text{D1})$$

and $\sigma'_{nm} = \sigma_{nm}$. From this result, we now define a gauge-invariant metric

$$g_{nm} = \gamma_{nm} - \beta_n \beta_m \quad (\text{D2})$$

where one can easily confirm $g'_{nm} = g_{nm}$ by using $\beta'_n = \beta_n - \partial_n \alpha$. We can think of γ_{nm} measuring the change of $|\psi(\theta)\rangle$ in the Hilbertspace, while g_{nm} measures its change excluding global phases which have no observable effect.

The quantum geometric tensor is defined as

$$\Xi_{nm} = \langle \partial_n \psi | \partial_m \psi \rangle - \langle \partial_n \psi | \psi \rangle \langle \psi | \partial_m \psi \rangle \quad (\text{D3})$$

and the QFIM as $\mathcal{F}_{nm} = \text{Re}(\Xi_{nm})$, which corresponds to the real part of g_{nm} .

The QFIM describes the change in fidelity for $|\langle \psi(\theta) | \psi(\theta + d\theta) \rangle|^2$ as we will see in the following. First, note that $\langle \psi | \partial_n \psi \rangle \in \text{Im}$. Thus, its derivative must be also imaginary, i.e. $\langle \psi | \partial_n \partial_m \psi \rangle + \langle \partial_m \psi | \partial_n \psi \rangle \in \text{Im}$, which immediately implies

$$\langle \psi | \partial_n \partial_m \psi \rangle = -\langle \partial_m \psi | \partial_n \psi \rangle. \quad (\text{D4})$$

Now, we find via Taylor expansion

$$\begin{aligned} \langle \psi(\theta) | \psi(\theta + d\theta) \rangle &\approx \\ 1 + i\langle \psi | \partial_n \psi \rangle d\theta^n + \frac{1}{2} \langle \psi | \partial_n \partial_m \psi \rangle d\theta^n d\theta^m &= \\ 1 + i\langle \psi | \partial_n \psi \rangle d\theta^n - \frac{1}{2} \langle \partial_n \psi | \partial_m \psi \rangle d\theta^n d\theta^m \end{aligned} \quad (\text{D5})$$

Now, we compute using Eq. (D5)

$$\begin{aligned} |\langle \psi(\theta) | \psi(\theta + d\theta) \rangle|^2 &= \\ \langle \psi(\theta) | \psi(\theta + d\theta) \rangle \langle \psi(\theta + d\theta) | \psi(\theta) \rangle &\approx \\ 1 - [\langle \partial_n \psi | \psi \rangle \langle \psi | \partial_m \psi \rangle] & \\ + \frac{1}{2} \langle \partial_n \psi | \partial_m \psi \rangle + \frac{1}{2} \langle \partial_m \psi | \partial_n \psi \rangle d\theta^n d\theta^m &= \\ 1 - \text{Re}[\langle \partial_n \psi | \partial_m \psi \rangle - \langle \partial_n \psi | \psi \rangle \langle \psi | \partial_m \psi \rangle] d\theta^n d\theta^m. \end{aligned}$$

where in the second step we used Eq. (D4). Finally, we have

$$|\langle \psi(\theta) | \psi(\theta + d\theta) \rangle|^2 = 1 - \frac{1}{4} \mathcal{F}_{nm} d\theta^n d\theta^m. \quad (\text{D6})$$

This implies that \mathcal{F} is a metric that describes the change in state space under a variation in parameter θ .

Appendix E: Data quantum Fisher information metric

We now generalize the QFIM to the DQFIM, which describes learning U with training states. We have a training set $S_L = \{|\psi_\ell\rangle, V|\psi_\ell\rangle\}_{\ell=1}^L$ and an ansatz $U(\theta)$. We learn using the cost function $C = 1 - L^{-1} \sum_{\ell=1}^L |\langle\psi_\ell|V^\dagger U(\theta)|\psi_\ell\rangle|^2$. Let us recall the projector onto the training data projector $\Pi_L = \sum_{k=1}^{B_L} |\phi_k\rangle\langle\phi_k|$ and its normalization $\tilde{\Pi}_L = \Pi_L/B_L$ where $|\phi_k\rangle$ are the eigenvectors with non-zero eigenvalue of $\rho_L = L^{-1} \sum_{\ell=1}^L |\psi_\ell\rangle\langle\psi_\ell|$ and $B_L = \text{rank}(\rho_L)$.

We now derive the DQFIM Eq. (E4) from a variational principle in a similar manner as the QFIM. The variation of isometry $U(\theta)\Pi_L/\beta$ with normalization factor $\beta = \sqrt{\text{tr}(\Pi_L)}$ is given by

$$\begin{aligned} ds^2 &= ||(U(\theta + d\theta) - U(\theta))\Pi_L/\beta|| = \text{tr}(\delta U^\dagger \tilde{\Pi}_L \delta U) = \\ &\text{tr}(\partial_n U^\dagger \tilde{\Pi}_L \partial_m U) d\theta^n d\theta^m = (\gamma_{nm} + i\sigma_{nm}) d\theta^n d\theta^m, \end{aligned}$$

where we have the difference $\delta U = U(\theta + d\theta) - U(\theta)$, the square of the Frobenius norm $||A|| = \text{tr}(A^\dagger A)$, the real and imaginary part γ_{nm} and σ_{nm} of $\text{tr}(\partial_n U^\dagger \tilde{\Pi}_L \partial_m U)$, and $\tilde{\Pi}_L = \Pi_L/\text{tr}(\Pi_L)$. Note that we have $\text{tr}(U^\dagger \tilde{\Pi}_L U) = 1$. One can now immediately check that one recovers the regular QFIM for $\rho_1 = |\psi\rangle\langle\psi|$. As ds^2 is hermitian, we have $\gamma_{nm} = \gamma_{mn}$ and $\sigma_{nm} = -\sigma_{mn}$, such that $\sigma_{nm} d\theta^n d\theta^m$ vanishes. However, γ_{nm} is not a proper metric as it is not invariant under the gauge transformation $U' = \exp(i\alpha)U$, i.e. a global phase rotation with α . We now construct a proper gauge invariant metric.

First, we apply ∂_n to $\text{tr}(U^\dagger \tilde{\Pi}_L U) = 1$ and see that $\text{tr}(\partial_n U^\dagger \tilde{\Pi}_L U) + \text{tr}(U^\dagger \tilde{\Pi}_L \partial_n U) = 0$. It follows that $\text{tr}(U^\dagger \tilde{\Pi}_L \partial_n U) + \text{tr}(U^\dagger \tilde{\Pi}_L \partial_n U)^\dagger = 0$ and thus $\beta_n = i\text{tr}(U^\dagger \tilde{\Pi}_L \partial_n U) \in \mathbb{R}$. Next, we compute $\text{tr}(U'^\dagger \tilde{\Pi}_L U') = \gamma'_{nm} + i\sigma'_{nm}$, where a straightforward calculation yields

$$\gamma'_{nm} = \gamma_{nm} + \partial_n \alpha \partial_m \alpha - \beta_m \gamma_n \alpha - \beta_n \gamma_m \quad (\text{E1})$$

and $\sigma'_{nm} = \sigma_{nm}$. From this result, we now define a gauge-invariant metric

$$g_{nm} = \gamma_{nm} - \beta_n \beta_m \quad (\text{E2})$$

where one can easily confirm $g'_{nm} = g_{nm}$ by using $\beta'_n = \beta_n - \partial_n \alpha$. We can think of γ_{nm} measuring the change of $U(\theta)$ in the full Hilbertspace, while g_{nm} measures the change excluding global phases which have no observable effect.

In analogy to the quantum geometric tensor, we define the data quantum geometric tensor

$$\Xi_{nm} = \text{tr}(\partial_n U^\dagger \tilde{\Pi}_L \partial_m U) - \text{tr}(\partial_n U^\dagger \tilde{\Pi}_L U) \text{tr}(U^\dagger \tilde{\Pi}_L \partial_m U) \quad (\text{E3})$$

and the DQFIM as $\mathcal{Q}_{nm} = \text{Re}(\Xi_{nm})$, which corresponds to the real part of g_{nm} , with

$$\mathcal{Q}_{nm}(S_L, U(\theta)) = 4\text{Re}(\text{tr}(\partial_n U^\dagger \tilde{\Pi}_L \partial_m U) - \text{tr}(\partial_n U^\dagger \tilde{\Pi}_L U) \text{tr}(U^\dagger \tilde{\Pi}_L \partial_m U)). \quad (\text{E4})$$

Indeed, we find for $L = 1$ that $\mathcal{Q}(S_1) = \mathcal{F}$. In contrast, for a training set with $\Pi_L = I$, we find what we call the unitary QFIM

$$\mathcal{Q}_{nm}^I = 4\text{Re}(d^{-1} \text{tr}(\partial_n U^\dagger \partial_m U) - d^{-2} \text{tr}(\partial_n U^\dagger U) \text{tr}(U^\dagger \partial_m U)). \quad (\text{E5})$$

The DQFIM describes the change of $|\text{tr}(U(\theta)^\dagger \tilde{\Pi}_L U(\theta + d\theta))|^2$ which we are going to show in the following. First, note that $\text{tr}(U^\dagger \tilde{\Pi}_L \partial_n U) \in \text{Im}$. Thus, its derivative must be also imaginary, i.e. $\text{tr}(U^\dagger \tilde{\Pi}_L \partial_n \partial_m U) + \text{tr}(\partial_n U^\dagger \tilde{\Pi}_L \partial_m U) \in \text{Im}$, which immediately implies

$$\text{tr}(U^\dagger \tilde{\Pi}_L \partial_n \partial_m U) = -\text{tr}(\partial_n U^\dagger \tilde{\Pi}_L \partial_m U). \quad (\text{E6})$$

Now, we find via Taylor expansion

$$\begin{aligned} \text{tr}(U(\theta)^\dagger \rho_L U(\theta + d\theta)) &\approx \\ 1 + i\text{tr}(U^\dagger \tilde{\Pi}_L \partial_n U) d\theta^n + \frac{1}{2} \text{tr}(U^\dagger \tilde{\Pi}_L \partial_n \partial_m U) d\theta^n d\theta^m &= \\ 1 + i\text{tr}(U^\dagger \tilde{\Pi}_L \partial_n U) d\theta^n - \frac{1}{2} \text{tr}(\partial_n U^\dagger \tilde{\Pi}_L \partial_m U) d\theta^n d\theta^m & \end{aligned} \quad (\text{E7})$$

Now, we compute using Eq. (E7)

$$|\text{tr}(U(\theta)^\dagger \tilde{\Pi}_L U(\theta + d\theta))|^2 =$$

$$\begin{aligned}
& \text{tr}(U(\boldsymbol{\theta})^\dagger \tilde{\Pi}_L U(\boldsymbol{\theta} + d\boldsymbol{\theta})) \text{tr}(U(\boldsymbol{\theta} + d\boldsymbol{\theta})^\dagger U(\boldsymbol{\theta})) \approx \\
& 1 - [\text{tr}(\partial_n U^\dagger \tilde{\Pi}_L U) \text{tr}(U^\dagger \tilde{\Pi}_L \partial_m U) \\
& + \frac{1}{2} \text{tr}(\partial_n U^\dagger \tilde{\Pi}_L \partial_m U) + \frac{1}{2} \text{tr}(\partial_m U^\dagger \tilde{\Pi}_L \partial_n U)] d\boldsymbol{\theta}^n d\boldsymbol{\theta}^m = \\
& 1 - \text{Re}[\text{tr}(\partial_n U^\dagger \tilde{\Pi}_L \partial_m U) - \\
& \text{tr}(\partial_n U^\dagger \tilde{\Pi}_L U) \text{tr}(U^\dagger \partial_m \tilde{\Pi}_L U)] d\boldsymbol{\theta}^n d\boldsymbol{\theta}^m.
\end{aligned}$$

where in the second step we used Eq. (E6). Finally, we have

$$|\text{tr}(U(\boldsymbol{\theta})^\dagger \tilde{\Pi}_L U(\boldsymbol{\theta} + d\boldsymbol{\theta}))|^2 = 1 - \frac{1}{4} \mathcal{Q}_{nm} d\boldsymbol{\theta}^n d\boldsymbol{\theta}^m, \quad (\text{E8})$$

which relates a change in parameter $\boldsymbol{\theta}$ to the change in the unitary projected onto the training states.

Appendix F: Degrees of freedom of isometries

Now, we calculate the degrees of freedom when learning a training set of L states with a d -dimensional unitary

$$U = \sum_{n,k=1}^d u_{nk} |n\rangle \langle k| \quad (\text{F1})$$

with $u_{nk} = a_{nk} + ib_{nk}$, where a_{nk} , b_{nk} are real parameters. First, note that U can be described using $2d^2$ real parameters, however due to $U^\dagger U = I$ and global phase, only $d^2 - 1$ real parameters are independent. We now compute the maximal number of degrees of freedom when U is projected onto a training set of L states. For any set S_L of training states, the rank of the projector Π_L is upper bounded by $\text{rank}(\Pi_L) \leq L$.

We apply U Eq. (F1) on a training set $\{|\ell\rangle\}_{\ell=1}^L$ of L states, where $|\ell\rangle$ are computational basis states. For a single training state $L = 1$, we have $U|1\rangle = \sum_{n=1}^d u_{n1} |n\rangle$. Via training, we can only learn the column vector $u_1 = (u_{11}, u_{21}, \dots, u_{d1})$, which has $2d$ real parameters and $2d - 2$ independent parameters due to constraints of global phase and norm $\sum_{n=1}^d |u_{n1}|^2 = 1$. However, all other column vectors besides u_1 cannot be learned. With the DQFIM we find $R_1 = 2d - 2$, i.e. R_1 indeed counts the number of degrees of freedom that can be learned. Next, we consider $L = 2$. Here, we additionally have the state $U|2\rangle = \sum_{n=1}^d u_{n2} |n\rangle$ and we can also learn the vector $u_2 = (u_{12}, u_{22}, \dots, u_{d2})$ with $2d$ real parameters. However, due to unitarity, u_2 must be orthogonal to u_1 , which removes two degrees of freedom. Additionally, we have to subtract one parameter for the norm condition. The global phase has already been incorporated in u_1 , thus u_2 holds $2d - 3$ degrees of freedom, with the $d \times 2$ -dimensional isometry (u_1, u_2) combined having $R_2 = 4d - 5$. For any L , each additional training state adds a column u_L , which has additional $2d - 2L + 1$ degrees of freedom due to $L - 1$ orthogonality conditions [69]. For L states, we have the isometry $U_L = (u_1, \dots, u_L)$, which can be described using

$$R_L = (2d - 2)L - (L - 1)^2 = 2dL - L^2 - 1 \quad (\text{F2})$$

real independent parameters and for $L \geq 1$. The maximum is reached for $L_c = d$ with $R_d = d^2 - 1$ and $U\Pi_d = U$ with $\Pi_d = I$, where we can completely learn U . For further increase in L we find that R_L stays constant. As our choice of U is a generic representation of a unitary and our chosen training set has maximal rank $\text{rank}(\Pi_L) = L$, our calculation gives us the upper bound for R_L . Note that by choosing a more constrained ansatz unitary and training sets R_L can be smaller.

For an arbitrary unitary, the gain in effective dimension by increasing dataset size $L \rightarrow L + 1$ is given by $\Delta R_L = R_{L+1} - R_L = \max(2d - 2L - 1, 0)$ for $L \geq 1$, and $\Delta R_0 = 2d - 2$ for $L = 0$. Thus, the gain decreases with L , i.e. with increasing L each additional state reveals less degrees of information of U .

Appendix G: Lie-algebra bounds DQFIM

Recall that our ansatz Eq. (A1) consist of G layers with

$$U(\boldsymbol{\theta}) = \prod_{k=1}^G U_k(\boldsymbol{\theta}_k) \text{ with } U^{(k)}(\boldsymbol{\theta}_k) = \prod_{n=1}^K \exp(-i\theta_{kn} H_n) \quad (\text{G1})$$

where $U^{(k)}(\theta_k)$ is the unitary of the k th layer. Here, H_n are K hermitian matrices and $\theta_k = \{\theta_{k1}, \dots, \theta_{kn}\}$ are the parameters of the k th layer. The total parameter vector $\theta = \{\theta_1, \dots, \theta_G\}$ of the ansatz has $M = GK$ parameters.

To simplify the notation, we treat each parameter entry as its own layer and relabel each generators H_k such that we can write the ansatz as

$$U(\theta) = \prod_{k=1}^M \exp(-i\theta_k H_k). \quad (\text{G2})$$

First, we define the generators of the ansatz U [37, 78]:

Definition 5 (Set of generators \mathcal{T}). *Consider ansatz Eq. (G2). The set of generators $\mathcal{T} = \{H_k\}_{k=1}^K$ (with size $|\mathcal{T}| = K$) are defined as the set of Hermitian operators that generate the unitaries of each layer of $U(\theta)$.*

Further the dynamical Lie Algebra \mathfrak{g} is given by:

Definition 6 (Dynamical Lie Algebra (DLA)). *Consider the generators \mathcal{T} according to Def. 5. The DLA \mathfrak{g} is generated by repeated nested commutators of the operators in \mathcal{T}*

$$\mathfrak{g} = \text{span} \langle iH_1, \dots, iH_K \rangle_{Lie}, \quad (\text{G3})$$

where $\langle \mathcal{S} \rangle_{Lie}$ is the Lie closure, which is the set obtained by repeatedly taking the commutator of the elements in \mathcal{S} .

Next, we show that the DLA bounds the rank of the DQFIM. First, let's recall the entries of the matrix of the DQFIM

$$\mathcal{Q}_{nm}(S_L, U(\theta)) = 4\text{Re}(\text{tr}(\partial_n U^\dagger \tilde{\Pi}_L \partial_m U) - \text{tr}(\partial_n U^\dagger \tilde{\Pi}_L U) \text{tr}(U^\dagger \tilde{\Pi}_L \partial_m U)). \quad (\text{G4})$$

where we shorten $U = U(\theta)$, $\tilde{\Pi}_L = \Pi_L / \text{rank}(\Pi_L)$ is the normalized projector onto the space spanned by the training states and $\partial_n U$ the derivative in respect to the n th element of parameter vector θ .

We now restate Theorem 1 for convenience.

Theorem 2. *The maximal rank R_L of the DQFIM is upper bounded by the dimension of the dynamical Lie algebra (DLA) $\dim(\mathfrak{g})$*

$$R_L \leq \dim(\mathfrak{g}), \quad (\text{G5})$$

where $\mathfrak{g} = \text{span} \langle iH_1, \dots, iH_K \rangle_{Lie}$ is generated by the repeated nested commutators of the generators H_k of the unitary $U(\theta)$.

The proof follows in analogy to the bound of the QFIM (i.e. R_1) of Ref. [37].

First, we note that $R_L \leq R_\infty$ as L simply increases the dimension of the projector Π_L . Now, we assume S_L spans the complete relevant Hilbertspace with $\Pi_L = I$ and thus we can simplify to the unitary QFIM

$$\mathcal{Q}_{nm} = 4\text{Re}(d^{-1} \text{tr}(\partial_n U^\dagger \partial_m U) - d^{-2} \text{tr}(\partial_n U^\dagger U) \text{tr}(U^\dagger \partial_m U)). \quad (\text{G6})$$

As we have $\partial_n \exp(-i\theta_n H_n) = -iH_n \exp(-i\theta_n H_n)$, we can write the derivatives as

$$\partial_n U(\theta) = -iU_{n+1 \rightarrow M} H_n U_{1 \rightarrow n}. \quad (\text{G7})$$

Here, we define

$$U_{m \rightarrow n} = U_n U_{n-1} \dots U_{m+1} U_m \quad (\text{G8})$$

as the propagator from layer m to layer n and

$$\tilde{H}_k = U_{1 \rightarrow k}^\dagger H_k U_{1 \rightarrow k}. \quad (\text{G9})$$

Using above expressions, we find for the first term of the DQFIM Eq. (G4)

$$\text{Re}(\text{tr}(\partial_n U^\dagger \partial_m U)) = \text{Re}(i(-i) \text{tr}(U_{1 \rightarrow n}^\dagger H_n U_{n+1 \rightarrow M}^\dagger U_{m+1 \rightarrow M} H_m U_{1 \rightarrow m})) = \text{Re}(\text{tr}(\tilde{H}_n \tilde{H}_m)).$$

Similarly, we find for the second term of Eq. (G4)

$$\text{Re}(\text{tr}(\partial_n U^\dagger U) \text{tr}(U^\dagger \tilde{\Pi}_L \partial_m U)) = \text{Re}(i(-i) \text{tr}(U_{1 \rightarrow n}^\dagger H_n U_{n+1 \rightarrow M}^\dagger U_{1 \rightarrow M})).$$

$$\text{tr}(U_{1 \rightarrow M}^\dagger U_{m+1 \rightarrow M} H_m U_{1 \rightarrow m}) = \text{Re}(\text{tr}(\tilde{H}_n) \text{tr}(\tilde{H}_m)).$$

We combine these results to get the DQFIM as

$$\mathcal{Q}_{mn}^I = \text{Re}(d^{-1} \text{tr}(\tilde{H}_n \tilde{H}_m) - d^{-2} \text{tr}(\tilde{H}_n) \text{tr}(\tilde{H}_m)) \quad (\text{G10})$$

Note that H_k are elements of the DLA \mathfrak{g} . As the unitaries U_n of the ansatz are also elements of the dynamical Lie group generated by \mathfrak{g} , a product of H_k with any U_n will yield another element of the dynamical Lie group. Thus, we can always expand H_k using the DLA as a basis with $\dim(\mathfrak{g})$ elements:

$$\tilde{H}_k = \sum_{m=1}^{\dim(\mathfrak{g})} a_m^{(k)} \chi_m, \quad (\text{G11})$$

where $a_m^{(k)}$ are real coefficients and $\{\chi_m\}_{m=1}^{\dim(\mathfrak{g})}$ are a basis of the DLA \mathfrak{g} . Thus, the matrix of the DQFIM \mathcal{Q} can be expressed in a basis with $\dim(\mathfrak{g})$ elements. Thus, the rank of \mathcal{Q} is upper bounded by the dimension of the DLA \mathfrak{g}

$$R_L \leq \text{rank}(\mathcal{Q}^I) \leq \dim(\mathfrak{g}). \quad (\text{G12})$$

Appendix H: Ansatz unitaries for SM

Next, in Fig.11 we show additional ansatz unitaries which are considered in the next sections of the SM.

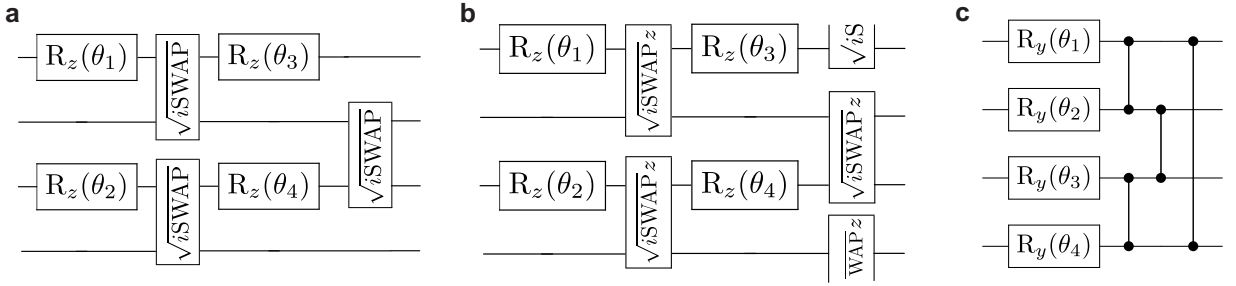


FIG. 11. Ansatz unitaries for the supplemental materials. The circuits are repeated for G layers. **a)** U_{XY}^{open} circuit with open boundary condition, i.e. the $\sqrt{i}\text{SWAP}$ do not cross from the first to the last qubit in contrast to U_{XY} . Commutes with particle number operator P and for sufficient depth can realize any time evolution generated by $\exp(-iH_{XY}^{\text{open}}t)$. **b)** U_{XXZ} circuit related to evolution of Heisenberg model H_{XXZ} . Composed of parameterized single qubit z rotations and the $\sqrt{i}\text{SWAP}z$ gate defined in the text. **c)** Real-valued ansatz U_{Y-CZ} consisting of y -rotations and control- Z gates in a nearest-neighbor chain configuration.

In Fig.11a we show the U_{XY}^{open} circuit, which is the same as the U_{XY} circuit but with open boundary conditions, i.e. the $\sqrt{i}\text{SWAP}$ gates that interact between the first and last qubit are removed. This ansatz conserves particle number P .

In Fig.11b we show the U_{XXZ} ansatz, which is composed of parameterized z rotations and the $\sqrt{i}\text{SWAP}z = \sqrt{CZ}\sqrt{i}\text{SWAP}$ gate, where $\sqrt{CZ} = \text{diag}(1, 1, 1, i)$ is the square-root of the control- Z gate. This ansatz conserves particle number P .

In Fig.11c we show the U_{Y-CZ} ansatz [48], consisting of parameterized y -rotations and control- Z gate $\text{diag}(1, 1, 1, -1)$. Due to its connection to Cluster-state generation, it overparameterizes with a polynomial number of parameters with $R_L \propto N^2$.

Appendix I: Generalization with further models

Here, we study the number of training states needed for generalization for further models.

First, in Fig.12a we study the U_{XY}^{open} ansatz shown in Fig.11a. This ansatz describes the evolution of the $H_{XY}^{\text{open}} = \sum_{k=1}^N h_k \sigma_k^z + \sum_{k=1}^{N-1} (\sigma_k^x \sigma_{k+1}^x + \sigma_k^y \sigma_{k+1}^y)$ Hamiltonian with open boundary conditions. The difference to H_{XY} is the absence of interaction between first and last qubit. We find generalization for $L = 1$ training states and $M \geq M_c$

when using random product states as training data. A similar ansatz was studied numerically in Ref. [10]. It was shown numerically that only 1 training state was needed for generalization, and $O(N^2)$ gates for successful training. Here, we explain this result with the DQFIM. In particular, our ansatz has the maximal rank of the DQFIM with $R_L = R_1 = R_\infty = N^2$ for all N . This implies that $L_c = 1$ training state is sufficient to get an overcomplete model and achieve generalization.

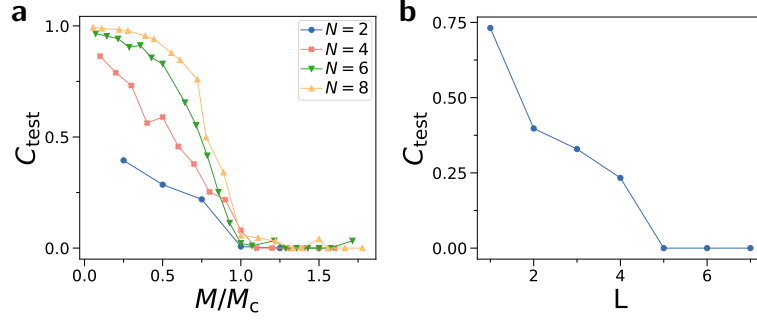


FIG. 12. **a)** Test error C_{test} for U_{XY}^{open} ansatz and for $L = 1$ product training states against circuit parameters M . C_{test} is averaged over 20 random instances. M_c is determined with the DQFIM. **b)** C_{test} for U_{XZZ} ansatz for product training states against L for $N = 4$ and $M = 100$.

Next, we study the U_{XZX} ansatz shown in Fig. 11b. This model can describes the evolution of the $H_{XZX} = \sum_{k=1}^N h_k \sigma_k^z + \sum_{k=1}^N (\sigma_k^x \sigma_{k+1}^x + \sigma_k^y \sigma_{k+1}^y + \Delta \sigma_k^z \sigma_{k+1}^z)$ Hamiltonian. A similar ansatz was studied in Ref. [10]. It was numerically shown that 5 training states are needed for generalization for $N = 4$. In Fig. 12b, we show the test error of the U_{XZX} ansatz against L in the overparameterized regime and indeed find the test error vanishes for $L \geq 5$. Using the DQFIM, we find $R_1 = 24$ and $R_\infty = R_{L_c} = 51$ with $L_c = 5$, matching the numerical results. Thus, the DQFIM accurately predicts the needed training states. Note that the approximation $L_c \approx 2R_\infty/R_1 = 4.25$ gives a good estimation of the number of needed training states as well.

Appendix J: Training of Y-CZ model

We show numerical results on training with the U_{Y-CZ} ansatz (see Fig. 11c for definition) in Fig. 13. This model requires $L = 2$ states to generalize as we have $R_L \sim N^2$. We find training and test error matches closely the transitions derived from R_L shown as black dashed lines.

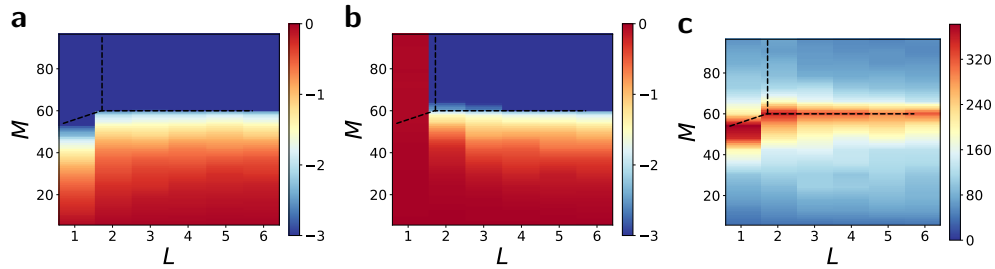


FIG. 13. Mean error for training U_{Y-CZ} for product state as training data and $N = 6$ qubits. **a)** C_{train} against M and L . Color shows logarithm $\log_{10}(C_{\text{train}})$. **b)** C_{test} against M and L . **c)** Number of training steps E until reaching $C_{\text{train}} < 10^{-3}$.